PAPER

Kinetic equilibrium reconstructions of plasmas in the MAST database and preparation for reconstruction of the first plasmas in MAST upgrade

IOP Publishing Plasma Physics and Controlled Fusion

Plasma Phys. Control. Fusion **63** (2021) 055014 (14pp) https://doi.org/10.1088/1361-6587/abf230

Kinetic equilibrium reconstructions of plasmas in the MAST database and preparation for reconstruction of the first plasmas in MAST upgrade

J W Berkery[1,*], S A Sabbagh[1], L Kogan[2], D Ryan[2], J M Bialek[1], Y Jiang[1], D J Battaglia[3], S Gibson[4] and C Ham[2]

[1] Department of Applied Physics and Applied Mathematics, Columbia University, New York, NY 10027, United States of America
[2] Culham Centre for Fusion Energy, UKAEA, Abingdon OX14 3DB, United Kingdom
[3] Princeton Plasma Physics Laboratory, Princeton, NJ 08543, United States of America
[4] Centre for Advanced Instrumentation, Durham University, Durham DH1 3LE, United Kingdom

E-mail: jberkery@pppl.gov

Received 24 December 2020, revised 10 March 2021
Accepted for publication 25 March 2021
Published 13 April 2021

Abstract

Reconstructions of plasma equilibria using magnetic sensors were routine during operation of the Mega Ampere Spherical Tokamak (MAST) device, but reconstructions using kinetic profiles were not. These are necessary for stability and disruption analysis of the MAST database, as well as for operation in the upgrade to the device, MAST-U. The three-dimensional (3D) code VALEN is used to determine eddy currents in the 3D vessel structures for vacuum coil test shots, which are then mapped to effective resistances in the two-dimensional vessel groupings in the EFIT equilibrium reconstruction code to be used in conjunction with nearby loop voltage measurements for estimated currents in the structures during reconstruction. Kinetic equilibrium reconstructions with EFIT, using all available magnetic sensors as well as Thomson scattering measurements of electron temperature and density, charge exchange recombination spectroscopy measurements of ion temperature, and internal magnetic field pitch angle measurements from a motional Stark effect (MSE) diagnostic are performed for a large database of MAST discharges. Excellent convergence errors are obtained for the portions of the discharges where the stored energy was not too low, and it is found that reconstructions performed with temperature and density measurements but without MSE data usually already match the pitch angle measurements well. A database of 275 kinetic equilibria is used to test the ideal MHD stability calculation capability for MAST. Finally, the necessary changes to conducting structure in VALEN, and diagnostic setup in EFIT have been completed for the upgrade from MAST to MAST-U, enabling kinetic reconstructions to commence from the first plasma discharges of the upgraded device.

Keywords: equilibrium reconstruction, stability, spherical tokamak

(Some figures may appear in colour only in the online journal)

* Author to whom any correspondence should be addressed.

1. Introduction

The Mega Ampere Spherical Tokamak (MAST) experiment was a low aspect ratio fusion plasma device that was used to study plasmas with high stability performance at low toroidal magnetic field [1]. Currently an upgrade to the device, called MAST-U [2], has begun operation. Accurate reconstruction of the plasma equilibrium state from various diagnostic measurements is crucial for the operation of MAST-U, as well as for the majority of plasma physics analyses including the stability analyses and disruption event characterization and forecasting (DECAF) [3, 4]. These last applications require kinetic equilibrium reconstructions, that is to say reconstructions using available measurements of the plasma pressure, for high accuracy.

Magnetic, kinetic, and rotating equilibrium reconstruction for low aspect ratio (A) ST plasmas has long been demonstrated [5]. MAST had, and MAST-U continues to have, world-class high resolution Thomson scattering measurements of electron temperature and density as well as charge exchange recombination spectroscopy measurements of ion temperature required for kinetic reconstructions. Additionally, in the present work, a pressure profile component due to energetic particles is allowed when reconstructing the total pressure profile. Internal magnetic field pitch angle measurements from motional Stark effect (MSE) diagnosis are also included for accurate determination of the safety factor, q, profile. The equilibrium reconstructions also include fitting of field shaping coil currents, and wall vessel currents (a critical component of reconstructions in low A plasmas due to the close presence of conducting elements in the device and the lower resistance of components in the centre of the device).

Reconstructions using a partial set of the magnetic measurements available during MAST operation, as well as a constraint on the last closed flux surface of the plasma through an optical measurement of $D\alpha$ radiation [6], were previously performed for each MAST discharge. These could then be used for database studies (as one example, see [7]). Reconstructions beyond magnetics–only were later performed individually for specialized studies, but were not uniformly available for the MAST database. For example, a limited number of kinetic equilibrium reconstructions with partial electron and ion pressure constraints and modelled fast ion pressures have been previously performed for MAST [8], but MSE measurements were not available at that time. Later, MSE was used to constrain the q profile for reconstructions otherwise using the inboard magnetics, but not the outboard magnetics or kinetic profiles [9]. A Bayesian inference technique, in which initial hypotheses of plasma parameters were made and the probability of those parameter values given the measured data were computed, was also pursued to compute MAST equilibria [10]. Finally, all diagnostics were brought together through a code suite called MC^3, which included magnetics, MSE, and finally total pressure, using the TRANSP particle transport analysis code [11] to determine the fast ion pressure component [12–14]. This level of equilibrium reconstruction was not routine, however, for MAST, and the present work presents an approach including internal plasma and field measurements to be used routinely for re-examination of the MAST database of discharges, as well as for operation of MAST-U. Additionally, the magnetics only level of reconstruction is recomputed here by using all available magnetics for comparison to reconstructions with internal plasma measurements. We find that that single D_α light constraint that was previously used as a boundary constraint is not needed in the present approach.

In section 2 the general concept of tokamak plasma equilibrium reconstruction is briefly reviewed, along with the specific equations solved here with various levels of diagnostic inclusion. Modelling of the conducting structure surrounding the plasma in the MAST device is discussed in section 3, with consideration of how this modelling leads to estimated induced currents in portions of the vessel which are then used in the reconstructions. The resulting reconstructions using magnetics only, kinetic, or kinetic plus MSE for MAST are compared in section 4 and used as a database for stability calculations in section 5. Finally, preparations for reconstruction of the first plasmas from MAST-U are outlined in section 6 and conclusions of the study are drawn.

2. Equilibrium reconstruction

A fusion plasma in a tokamak is said to be in equilibrium when a steady–state force balance in the radial and vertical directions is in effect. The state of this equilibrium for a given discharge at a given time can be reconstructed from various measurements and this provides integrated plasma characteristics such as stored energy, or profile information such as safety factor. The EFIT code is an equilibrium reconstruction code for tokamak plasmas [15–17]. While one particular implementation of the EFIT code with a C++ data flow layer which also incorporates a model of the induced currents [18] as a pre-processing step, called EFIT++ [19, 20], has been used for MAST reconstructions in the past, another implementation, previously used for the NSTX [5] and KSTAR devices, is now being used for MAST reconstructions in the present work. Both of these codes will be used for MAST-U operation, as will be discussed in section 6.

The equilibrium of a tokamak plasma satisfies a balance of current and pressure forces, $\nabla p = j \times B$. In 2D axisymmetry, this results in the Grad–Shafranov equation,

$$R^2 \nabla \cdot \left(\frac{\nabla \psi}{R^2} \right) = -\mu_0 R J_\varphi,$$

where the toroidal plasma current is defined by,

$$\mu_0 J_\varphi = \mu_0 R \frac{\partial p}{\partial \psi} + \frac{f}{R} \frac{\partial f}{\partial \psi},$$

with p the total plasma pressure and $f = RB_\varphi$. Reconstruction of the plasma equilibrium requires the specification of two functions and a boundary specification, which experimentally is self-consistently determined by the combination of current in the plasma and a set of external magnetic coils. Normally one selects $\partial p/\partial \psi$ and $f \partial f/\partial \psi$.

The function $f\partial f/\partial\psi$ is a function of ψ_N only, where ψ_N is the poloidal flux normalized so that it spans 0:1 from axis to edge. We use a polynomial basis set of order n_f to specify $f\frac{\partial f}{\partial\psi} = \sum_0^{n_f} \gamma_n \psi_N^n$, and at this point constraints are placed on the equation to avoid large degeneracies in the solution due to the profiles having too much freedom given a certain set of input measurements. Previous work [5] has shown that a constraint needs to be set for the $f\partial f/\partial\psi$ function at the plasma edge. Setting a Dirichlet boundary condition $f\partial f/\partial\psi = 0$ is possible, but it is too restrictive in that it suggests no current at the edge from this function. A constraint that has been shown in past work [5] to be superior is the Neumann boundary condition,

$$\left[\frac{\partial}{\partial\psi}\left(f\frac{\partial f}{\partial\psi}\right)\right]_{\psi_n=1} = 0\,.$$

This works well in that it is a free-end boundary condition allowing the poloidal currents to be finite at the edge, yet it constrains the profile sufficiently to largely avoid solution degeneracy. This can be achieved by stipulating that the γ parameters should abide by the constraint $C_0 \sum_1^{n_f} n\gamma_n = 0$, where C_0 is an arbitrary constant. This same constraint on $f\partial f/\partial\psi$ is used in all levels of reconstruction.

Data constraints are applied in the EFIT code by adding additional equations along with diagnostic measurements in the form, $D(t) = R \times U(t)$. Here D represents the diagnostic measurements, R the response matrix including currents in the plasma and vessel, and the Green's function for the poloidal field coil currents, and U contains the free parameters. This system is solved by least squares regression, minimizing the χ^2 between the measured quantities, M, and those calculated by $R \times U$, C. Specifically, $\chi^2 = \sum (M_i - C_i)^2/\sigma_i{}^2$, where σ_i is the uncertainty of each data measurement. The constraints then, despite their name, are therefore not strictly enforced. A weighting between the importance of the diagnostic elements is determined by the error associated with each element. The constraints related to the profile forms mentioned here are given relatively low weighting so that the influence of the measurements dominate the χ^2 minimization.

The second function, the pressure gradient $\partial p/\partial\psi$, is also treated as a polynomial of order n_p: $\frac{\partial p}{\partial\psi} = \sum_0^{n_p} \alpha_n \psi_N^n$, and similarly, a constraint is placed on this equation. We set the pressure gradient at the axis equal to zero, so that $\alpha_0 \approx 0$.

The two functions are treated with varying polynomial orders n_f and n_p, as well as one additional constraint at the kinetic reconstruction level, leaving different numbers of free parameters, depending on the measurements used as inputs. Selection of the polynomial orders is a trade-off between a larger value allowing more detail in the profiles but also introducing more unknowns to the reconstruction and unacceptable levels of solution degeneracy. Increased degeneracy leads to more difficulty in the solution algorithm convergence, yielding increased convergence error. Each level of analysis will now be described in greater detail.

2.1. Magnetics only reconstruction

Magnetic diagnostics [21] are used in all levels of equilibrium reconstruction. At its most basic level, an equilibrium reconstruction can be successful using magnetics data only, without any internal plasma profile measurements. The MAST device was fully equipped with magnetic diagnostics, including Rogowski coils, pickup coils, and flux loops used for this purpose [22].

In the magnetics only case, because no pressure measurements are available, we treat the total plasma pressure gradient as a polynomial flux function with the relatively low order of $n_p = 2$. Additionally, because we have specified a pressure gradient of zero at the axis, we can reduce the expression to $\partial p/\partial\psi \approx \alpha_1\psi_N + \alpha_2\psi_N^2$, and for the magnetics only reconstruction we will also specify a pressure gradient of zero at the edge. Note that to allow finite toroidal current at the plasma edge, which is found to be required to reconstruct plasmas during periods of strong edge currents [5], the $f\partial f/\partial\psi$ function is allowed to be finite at the plasma edge. Finally, a weak constraint is set to guide the reconstruction to have zero plasma pressure at the plasma boundary, but again this condition is not strictly set. We then fit $\partial p/\partial\psi$ to,

$$\frac{\partial p}{\partial\psi} \approx \alpha_1\psi_n(1-\psi_n)\,,$$

and the resulting pressure profile conforms to

$$p \approx p_0\left(1 - 3{\psi_n}^2 + 2{\psi_n}^3\right),$$

where p_0 is the pressure on axis, providing a cubic shape which arguably allows reasonable inflection in the pressure profile without forcing solutions to large edge pressure gradients, if not warranted by the measurements.

To have the greatest reconstruction fidelity to the equilibrium profiles expected, it is desirable to allow the greatest amount of profile freedom for a given measured data set. The present model allows the pressure profile to be third order in ψ, allowing profiles that can have small gradients on axis and at the boundary. The constraints on pressure listed above then yield a pressure profile shape with one free parameter, p_0. For the poloidal current function the order for $f\partial f/\partial\psi$ of $n_f = 4$ is used, without additional constraints, besides the derivative of $f\partial f/\partial\psi$ equal to zero at the edge listed above. This yields a total of four free parameters for the equilibrium functions. While standard aspect ratio plasmas allow two free parameters, and plasma shaping breaks solution degeneracy to allow three free parameters [15], in external magnetics only reconstructions, it has been found that four free parameters can be allowed in the equilibrium profile models for low aspect ratio plasmas [5].

The higher order polynomials used for STs have the advantage of flexibility in reconstructing greater profile detail, but the potential weakness is to allow too much freedom to the profiles, which could make it difficult to get a converged solution. The constraints help to reduce that freedom by guiding the reconstruction to physically reasonable, converged solutions that do not stray into exotic or unphysical profile

shapes. The constraints that were used in this work (and for NSTX), with their relatively low weights, were found to be effective for ST reconstructions. It should be noted that due to the relatively low weight given to these extra constraints, they are not strictly met in the reconstruction, as that is not their purpose.

2.2. Partial kinetic reconstruction

In addition to magnetics data, the next level of reconstruction uses the Thomson scattering profiles of electron density and temperature [23, 24], and the charge exchange recombination spectroscopy profile of ion temperature [25] to constrain the pressure profile [16]. This reconstruction is called 'partial kinetic' because the ion density and the fast particle pressure are not directly measured. In this case, the ion density is assumed to be equal to the electron density times a constant less than one—here we found 0.7 to give good results—to account for the presence of impurity ions. The ion pressure is given an associated error bar in the fitting procedure because of the uncertainty due to this assumption. A trustworthy measurement of the plasma effective charge state, $Z_{\rm eff}$ [26], would be useful to give a better estimate of ion density. The fast particle pressure, which can also constitute a significant portion of the total pressure, is here taken to be equal to the electron pressure, and assigned a very large error ($\sim$100%) to allow sufficient freedom in the total pressure profile fitting to the data. Reconstruction with this partial level of kinetic measurement input, however, is commonly referred to simply as kinetic reconstruction. One reason is because the fast particle pressure is never directly measured, so when included, it is at best modelled.

As mentioned, assumed 'measured' profiles of ion and fast particle pressures are used, with large error bars to allow flexibility in the total pressure profile. It would also be possible to couple the reconstruction to a transport code [27], or to use the original equilibrium as an input to a transport calculation which provides a calculated $p_{\rm f}$ profile. Then this profile could be used as a 'measured' input (again with large error bars because it is not a truly measured quantity) in the equilibrium reconstruction, and the process could be iterated until reasonable convergence is obtained. Alternatively, a neural network emulation of the results of TRANSP calculations could also be used to approximate the fast ion pressure again based on modelling [28]. These steps have not yet been taken in the present analysis.

Because the pressure profile is being constrained by more measurements in kinetic reconstructions, it is possible to give more freedom to the fit for $\partial p/\partial\psi$. For all kinetic reconstructions, we have used a polynomial order of five and the zero gradient constraint at the axis (but not at the edge, like in the magnetics only case). Finally, we also used $n_{\rm f} = 5$ for $f\partial f/\partial\psi$, but in addition to the previously described Neumann constraint, we now also specify that the value of $f\partial f/\partial\psi$ is zero on axis as well, which is achieved by setting $\gamma_0 \approx 0$. These are the same settings used for kinetic reconstructions in NSTX [29]. The weights on these constraints are relatively weak compared to the weighting of the match to the data (set by the data error bars alone), and in the cases shown here the solution does not strictly obey them, allowing a finite toroidal current at the axis, as will be shown.

2.3. Partial kinetic reconstruction with MSE

Besides the density and temperature measurement inputs, at this stage of reconstruction, magnetic field pitch angle data, measured by the MSE diagnostic, can also be used. The MSE diagnostic for MAST [30, 31] is used to find the polarization angle of light emitted from neutral beam particles in the local magnetic field of the plasma. The polarization angle is self-consistently converted to the magnetic pitch angle using the magnetic field components during the iterative steps of our equilibrium reconstruction. Naturally, the magnetic pitch angle measurement, the only magnetic measurement internal to the plasma, serves as a strong constraint on the q profile in the plasma, q being a measure of the ratio of magnetic field components. Adding MSE provides a better constraint to the equilibrium reconstruction, but no changes to the order or constraints for $\partial p/\partial\psi$ or $f\partial f/\partial\psi$ are made at this step.

MSE-constrained equilibria are important especially for magnetohydrodynamic (MHD) stability studies, in which case knowledge of the q profile, and especially its value at the magnetic axis, q_0, is critical. An example from MAST is the study of the so-called long-lived mode, which evolves as q_0 approaches, but stays above, one [9].

Finally, reconstructions including plasma rotation are also possible [17, 29, 32–34], but have not been performed for MAST or MAST-U plasmas in this work. The effect can especially significant in the spherical torus due to the low aspect ratio of the plasma as shown in NSTX reconstructions that include toroidal rotation [29]. For MAST, it has been speculated that disagreement between the inboard and outboard temperature and density profiles could be indicating a rotational shift of the flux surfaces [8]. Indeed, the importance of flow in radial force balance was previously demonstrated for a single MAST discharge/time point [32]. The measurement capabilities do make this level of analysis possible, and the generally high levels of toroidal rotation in STs with neutral beam injection (NBI) providing torque [35] justifies such analysis for future work.

3. Modelling of the MAST conducting structure supporting equilibrium analysis

For equilibrium analyses of spherical tori it is important to include currents in the conducting structure of the tokamak modelled, as their influence will dominate the toroidal current during plasma current ramp-up, and will comprise a significant component of the plasma current well into the $I_{\rm p}$ flat-top period of the discharge [5]. To obtain the best set of effective resistances of the wall segments for equilibrium reconstruction, we have created a three-dimensional (3D) non-axisymmetric model of the wall, including the centre column, the coil cases, and the vacuum vessel with ports, using the VALEN code [36]. The VALEN code approximates the conducting structure

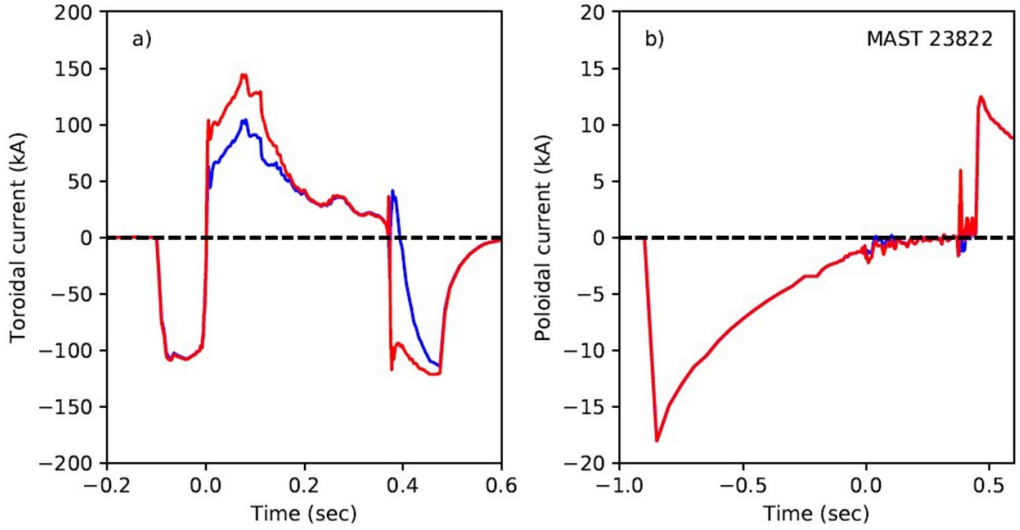

Figure 1. (a) Total induced toroidal current and (b) poloidal current in the MAST conducting structure with (blue) and without (red) plasma current for discharge 23822, as calculated by VALEN. Note the different time and current scales for each plot.

surrounding the plasma by splitting a thin-shell into finite elements which are each mutually coupled to all other elements in the model. Then, when some currents in the system are specified, currents that are induced in the conducting structure can be identified.

As a first test of this capability for MAST, time-domain calculations were performed using experimental currents in coils with and without plasma current for MAST discharge 23822. As an approximation, the plasma current was uniformly distributed in a circular cross section at the experimental major and minor radius. Figure 1 shows the resulting net toroidal and poloidal currents in the conducting structure of MAST. As expected, the toroidal current in the conducting structure is reduced when plasma current is present. For comparison, the flat-top plasma current in this discharge was ∼750 kA, so the induced current is significant. The toroidal current is induced by the changing poloidal field coil currents, especially the +22 to −17 kA swing in the P1 Ohmic solenoid in the centre case. The much smaller (note the scale in figure 1(b)) poloidal conducting structure current, which is essentially zero during the plasma discharge time of ∼0–0.4 s, is induced by the slower toroidal field coil current ramp to and from −86 kA. Figure 2 shows the eddy current pattern in the MAST conducting structure when the plasma is present and the toroidal current dominates. The size of the arrows indicates the strength of the current in each segment of the structure. One can see the pattern of the current is mostly toroidal, with some current flowing around vacuum ports.

Measurements of the currents in some plasma facing wall components, namely the coil cases, were available during MAST operation. These were measured by the difference between Rogowski coil measurements of the current through the coils plus cases, and the coils alone, measured at the leads. There is considerable noise in the measured signal due to it actually being the difference between two large signals. An example of a comparison between these measured currents and

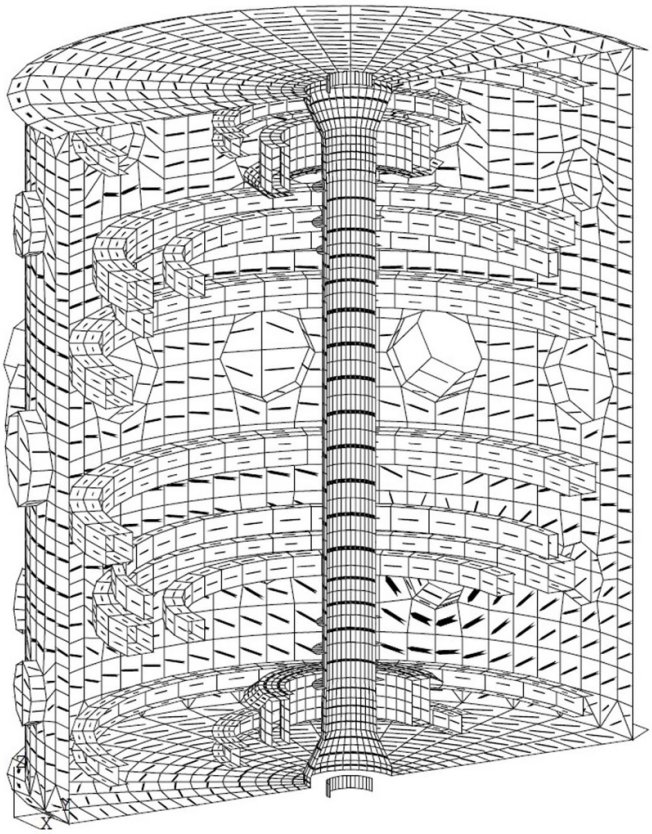

Figure 2. View of the eddy current pattern in the MAST conducting structure during plasma discharge 23822.

the current isolated to that particular coil case in the VALEN model is shown in figure 3.

The close match of the coil case current comparison gives confidence in the VALEN model. That model is now used to approximate the current in other, unmeasured, vessel segments

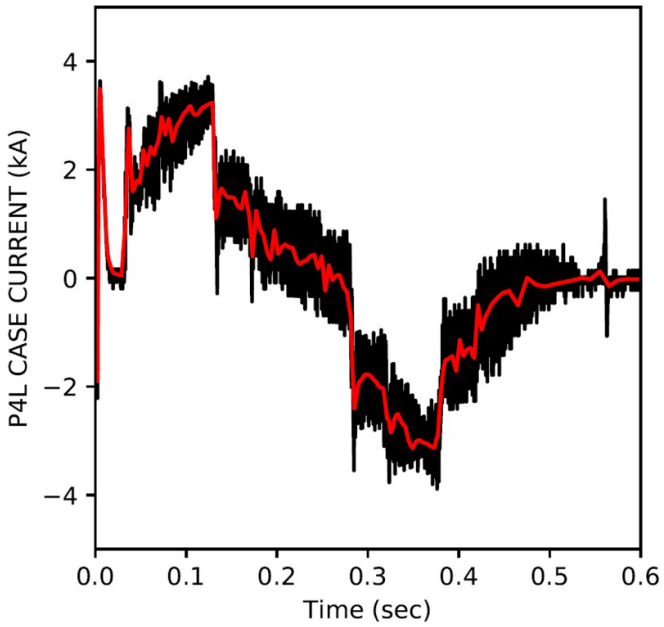

Figure 3. Comparison between measured (black) and VALEN modelled (red) induced currents in the lower P4 coil case during MAST poloidal field coil test discharge 23588.

for the equilibrium reconstruction. A similar, though strictly 2D, procedure was previously used for MAST reconstructions [18]. First, we have divided the MAST conducting structure into 14 axisymmetric toroidal segment groupings, plus an upper and lower divertor plate near poloidal field coils P2. Additionally, the P6 coil cases are treated as vessel segments with unknown current levels, as their currents were not measured. This total of 18 vessel segments without experimentally measured current is shown in figure 4(a) (the flux surfaces from an equilibrium reconstruction are also included—these will be discussed in section 4, and the MAST-U diagram in figure 4(b) will be discussed in section 5). Only stainless steel and Inconel components are shown, carbon tiles are not. There is a trade-off between having too few or too many modelled vessel segments. Too few will mean that the reconstruction cannot sufficiently capture the poloidal distribution of current in the vessel to accurately match the magnetics, while too many gives the equilibrium reconstruction too much freedom to distribute the current, resulting in degenerate solutions.

By grouping the VALEN elements into the same segments, the total induced current flowing in each of those segments can be determined. While, theoretically, one could run VALEN iteratively as a part of the reconstruction of each discharge, using the modelled currents in the vessel segments from VALEN directly, it is much more practical to use VALEN modelling to calibrate a measured signal to use as an estimated current. Each of the segments, then, is paired with a nearby measurement of loop voltage which, when coupled with an effective resistance of the segment grouping as a whole, will provide an estimate of the total current in that segment [5]. The current in each segment is distributed evenly throughout its cross-sectional area in the reconstruction. The resistances of the vessel segments can also be modelled by considering the cross sectional area, circumferential length, and material resistivity of the segments and considering each piece of the segment to be in a parallel circuit. For a simple geometry segment, such as VS1U (the red centre stack casing section in figure 4), with a loop voltage measurement at the same location (right on the centre stack), this method compares well to the VALEN effective resistance determination: 1.90×10^{-4} vs. 1.86×10^{-4} Ohms. However, for a more complex geometry, such as the three distinct parts of VS3U (green in the upper left of figure 4), and when the nearest available loop voltage measurement is farther away (at the bottom left corner of the P2 coil case in this case), there can be a sizable difference between the geometric modelled and VALEN determined effective resistances: 2.30×10^{-5} vs. 4.17×10^{-5} Ohms, in this case, proving the necessity of the further calibration step using VALEN.

VALEN is used to compare predicted currents in the vessel segments for a few discharges to those derived from the loop voltage measurements, thereby verifying/calibrating the effective resistances to use for further equilibrium reconstructions. An example comparison is shown in figure 5 for poloidal field coil test discharge 23588 (no plasma) of the current in vessel segment 7U, above the outboard midplane (the upper half of the orange segment in figure 4(a)). Plotted are the VALEN modelled current and the signal from loop voltage monitor P5U4 divided by the determined effective resistance of the segment, determined through this process to be 1.875×10^{-5} Ohms. Good agreement is found.

4. Comparison of various levels of equilibrium reconstruction for MAST

Once the sources of current are included as described in the previous section, from both applied current in coils and estimated induced current in vessel structures, various levels of diagnostic data can be input, as described in section 2. A solution to fit the diagnostic data is iterated until a low convergence error is obtained. In this section, we show some examples of various quantities for MAST plasmas with the different levels of equilibrium reconstruction. For the magnetics-only level, the available diagnostics were up to 16 raw loop voltage signals, 10 hardware-integrated flux loops on the centre column and 36 spaced around the vessel poloidally, 40 centre column pickup coils measuring vertical field, and 19 pickup coils on the outboard side measuring vertical field and 19 measuring radial field. In practice, by the later stages of MAST operation, a number of those probes were not operational, but a large number remained to provide a good magnetic reconstruction. In the kinetic reconstruction, 130 channels of Thomson scattering measurements of the electron temperature and density, as well as 64 channels of charge exchange recombination spectroscopy are added, as described in section 2.2. Finally, at the kinetic plus MSE level up to 35 channels of polarization angle from the MSE diagnostic are included, as described in section 2.3.

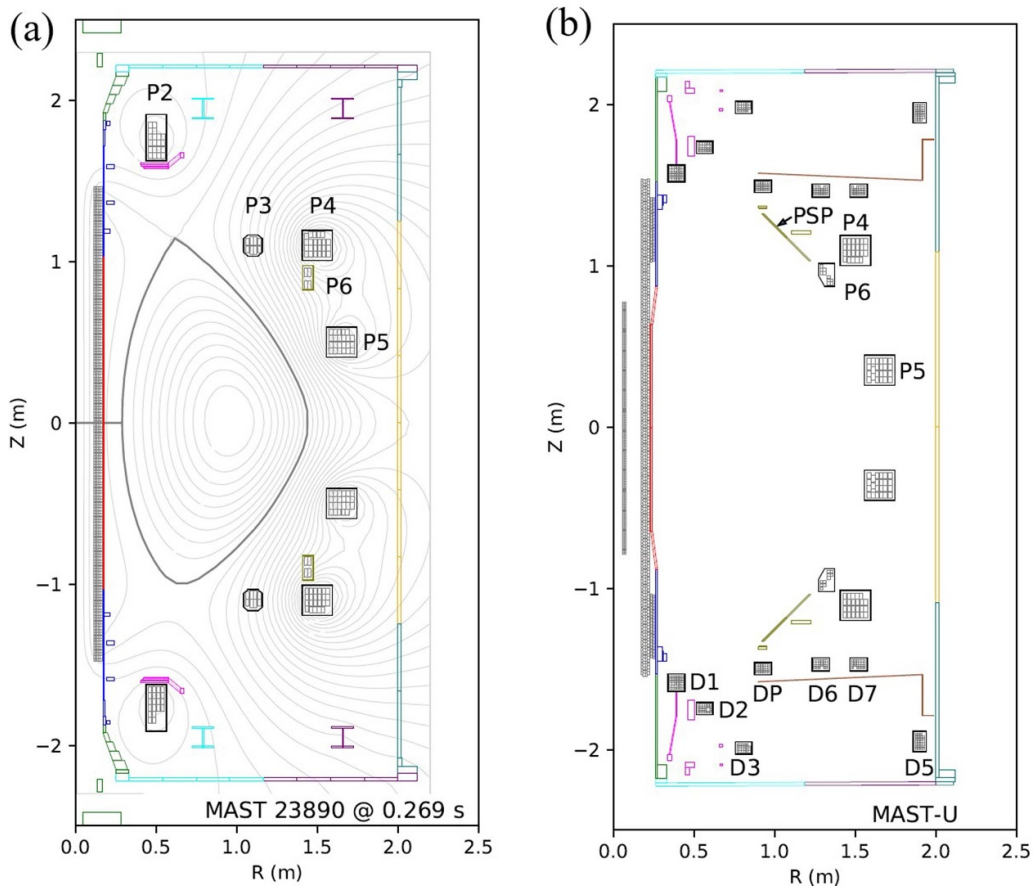

Figure 4. Diagrams of (a) MAST, and (b) MAST-U poloidal field coils (grey), their cases (black), and all toroidally continuous conducting vessel structures (colours), as well as the flux surfaces of an example plasma equilibrium reconstruction for MAST in (a). There are a total of 18 vessel segments in the MAST model, including the P6 cases and the divertor plates near P2. There are 20 for MAST-U including the colosseum structure outside of D1-3, the gas baffle outside of DP6-7, and the passive stabilization plates between DP and P6. Colours are reused for upper and lower segments to show symmetry, but these segments are considered separately, including two inner wall segments in red and two outer wall segments in orange, each split at the midplane into upper and lower parts.

Figure 6 shows a comparison of the reconstructed pressure and magnetic pitch angle profiles at the midplane from the three levels of reconstruction for an example case of MAST discharge 23890 at 0.269 s. This is the same discharge and time for which the flux surfaces were shown in figure 4(a) (from the kinetic plus MSE level). One can see differences in the profiles between the three levels of analysis. The change in pressure profile shape allowed by the higher level of polynomial order for the kinetic fits is clear. Note that in this particular case the kinetic (blue) and kinetic plus MSE (red) are so similar they nearly identically overlay in the figure.

Note that the 'measured' pressure profile in figure 6 is only partially measured, and partially modelled, as described in section 2.2. It is also worth noting that while the Thomson scattering measurement of electron pressure spans the full midplane cross section of the plasma (in great detail, with 130 points), the charge exchange recombination spectroscopy measurement of the ion temperature spans from 0.78 m outward. The modelled data points for total pressure, shown in figure 6 with large error bars, therefore have two sections, one where n_i and p_f need to be assumed and another where additionally, T_i is assumed (equal to T_e). These regions are not distinctly noticeable in figure 6, however, partly due to the large error bars.

We also note that the measured pressure profile (grey) was not available to the magnetics only reconstruction in green on the top panel of figure 6. Similarly, the MSE measured magnetic pitch angle data (grey) was not available to either the magnetic (green) or kinetic (blue) reconstructions in the bottom panel. In spite of that, those levels of reconstruction actually do quite well compared to the MSE data already, before it is even included. The kinetic with MSE level of reconstruction actually does not greatly refine the kinetic profile in this case, because the kinetic reconstruction of pitch angle already fell within the error bars of the MSE measurement. This can be seen as well in the q profile for each level of reconstruction, shown in figure 7, vs. normalized Ψ. The q profiles are all similar, but the kinetic cases differ slightly in the core where they have available measurements to constrain the fit but the magnetics-only case does not. The two kinetic levels of reconstruction are almost identical throughout the discharge, as can be seen in figure 8, which shows the stored energy vs. time. It should be noted that the q profile is monotonic in this case. It will also be useful to perform this

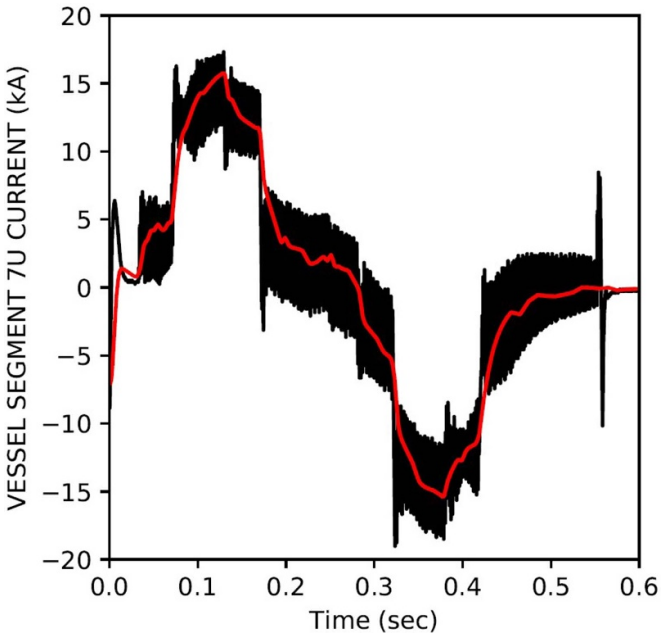

Figure 5. Comparison between measured loop voltage divided by effective resistance (black) and VALEN modelled (red) induced currents in the vessel segment 7U (above the outer midplane) during MAST poloidal field coil test discharge 23588.

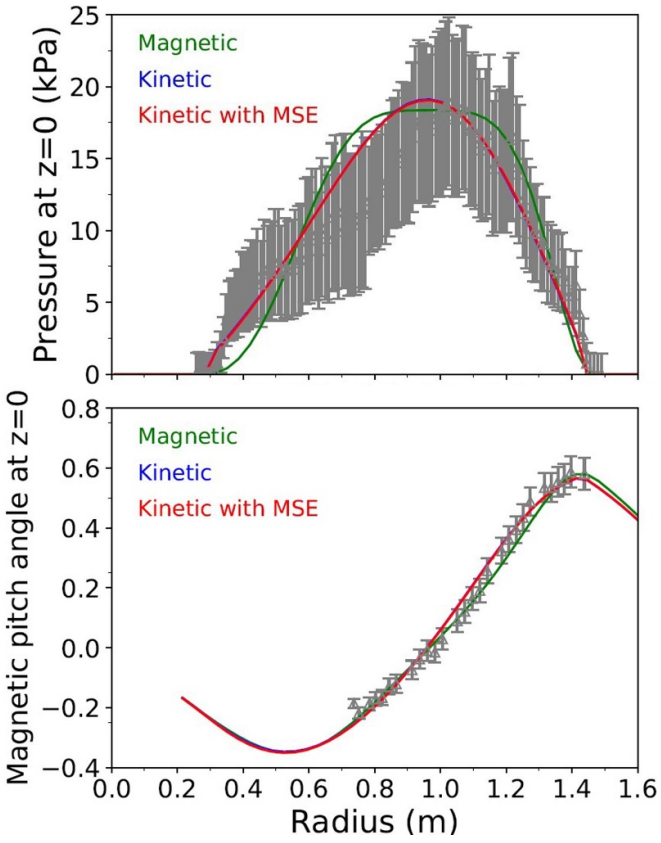

Figure 6. (Top) Pressure and (bottom) magnetic pitch angle (in radians) profiles vs. radius at $z = 0$ for MAST discharge 23890 at 0.269 s. Three levels of equilibrium reconstruction are compared to the measured profiles (the pressure profile being partially measured and partially modelled).

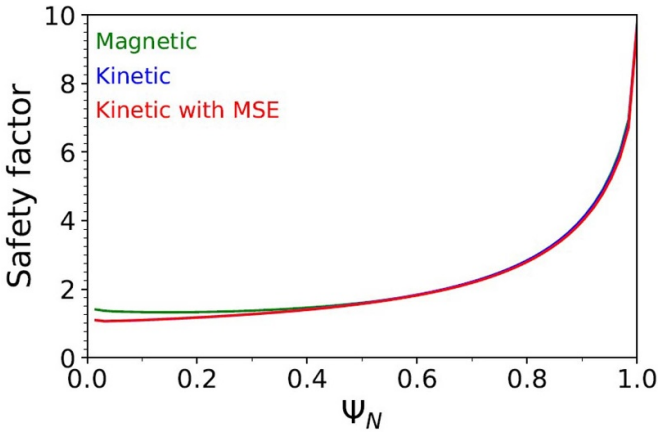

Figure 7. Q profile vs. normalized Ψ for MAST discharge 23890 at 0.269 s.

analysis on equilibria with reversed shear q profiles, where including the MSE data is expected to have an increased impact upon the reconstructed q profile (for example in figure 3 of [30]).

Noticeable differences between the magnetic and kinetic reconstructions, as seen by the difference in stored energy, occur both during the early phase of the plasma (∼0.1 s) and the current flattop. In the early phase the kinetic profiles have relatively small values and the kinetic reconstruction does not perform as well. During the current flattop, inclusion of kinetic profiles helps refine the reconstruction, showing a somewhat lower value of stored energy than the magnetics-only case.

One method of determining how good the reconstruction is, is to examine the convergence error of solving the Grad-Shafranov equation for the poloidal flux, Max $\left|{\psi_n}^{m+1} - {\psi_n}^{m}\right|$, where m is the iteration step. The convergence error metric shows how well the equilibrium solution is converging to one solution, as opposed to alternating between multiple solutions possible within the given constraints, for example. These are shown for MAST discharge 23890 vs. time in figure 8, including markers at time 0.269 s, when the profiles from figures 6 to 7 were taken from. Based on needs for subsequent MHD stability analysis, the required convergence error should be at least 1×10^{-4}, which we see is well satisfied for most of the equilibria computed outside of the plasma current ramp-up and discharge formation in the vessel. The levels below 10^{-6} during the high stored energy part of the discharge are excellent. Additionally, the kinetic reconstructions are seen to perform better than the magnetics only during this portion of the discharge. As expected at certain times, adding MSE will increase the convergence error in cases where the full complement of external magnetics, pressure and pitch angle constraints may have certain small inconsistencies (for example the spike in the bottom plot of figure 8 at ∼0.26 s). This usually occurs due to underestimates of the error bars for the individual diagnostic channels. Further analysis over greater ensembles of plasmas will reveal repeated small inconsistencies, and is a robust procedure for finding that somewhat larger error bars are required

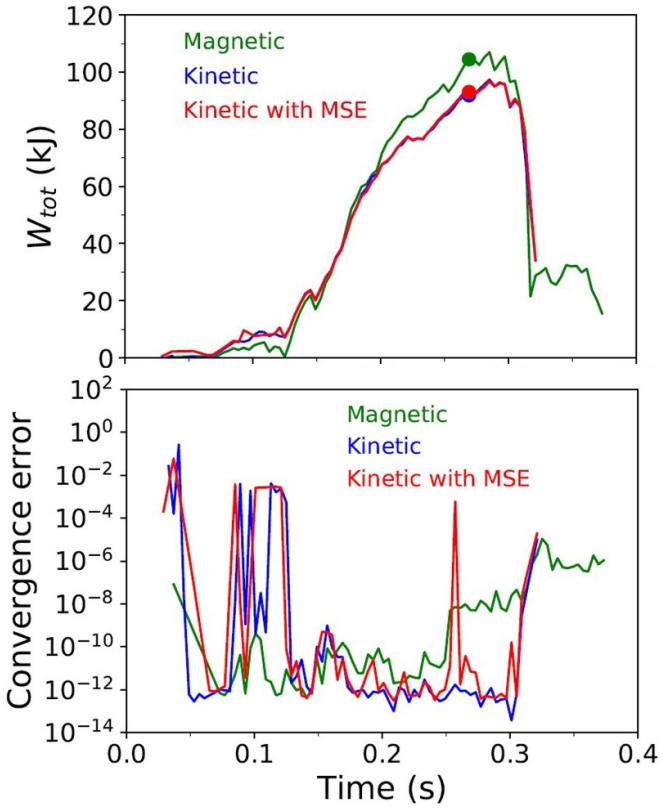

Figure 8. (Top) Stored energy, and (bottom) convergence error vs. time for three levels of equilibrium reconstruction for MAST discharge 23890.

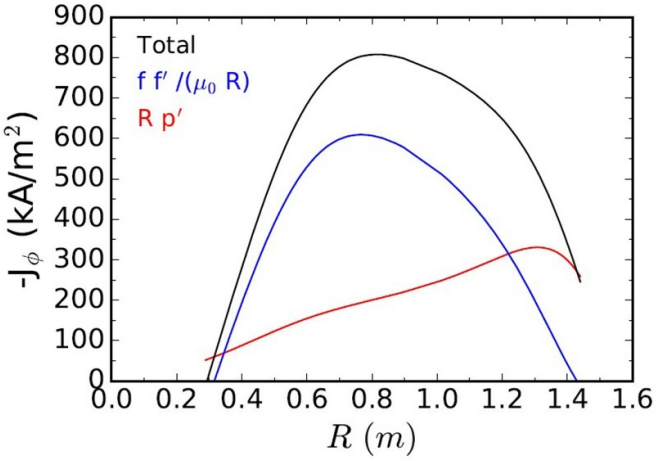

Figure 9. The total, and components of $-\boldsymbol{J}_\varphi$ for the kinetic reconstruction of MAST 23890 at 0.269 s (the current is negative in MAST by convention).

for certain channels (e.g. due to drifts in magnetic signals, stray light in MSE channels, etc…).

Secondly, the χ^2 function is the key figure of merit showing the goodness of fit for an equilibrium reconstruction. Based on the definition of χ^2, we should expect that if all of the errors considered for each data point represented accurate Gaussian statistics for each measurement, the reconstruction should have an expected value of $\chi^2/N_\mathrm{M} = 1$, where N_M is the number of measurements used in the reconstruction. For the MAST discharge 23890 shown in figure 8, after about 0.15 s we find that the magnetics only reconstruction has a steady value of about $\chi^2/N_\mathrm{M} \approx 3$ when using all 136 magnetic signals. However it was noticed that five of these magnetic probe signals disagree with the reconstructed values somewhat outside of the error bars, and they account for a significant component of the χ^2 value, indicating a discrepancy between the magnetics, or an inconsistency with the model. This is a standard result that often leads to corrected probe compensation by the diagnostician, or alteration of the model. If this small percentage of probes is excluded from the reconstruction process, then $\chi^2/N_\mathrm{M} \approx 1.5$. The kinetic reconstructions, which add 130 pressure profile measurements with large error bars, has a $\chi^2/N_\mathrm{M} \approx 1.5$ with all magnetics included.

It is useful now to examine the solution for the toroidal current density, J_φ, and its two components, $R(\partial p/\partial\psi)$ and $(f\partial f/\partial\psi)/(\mu_0 R)$. For this we again turn to the example discharge 23890 at 0.269 s, shown for the kinetic reconstruction in figure 9. One can see the detail in the profiles allowed by the fifth order polynomials. The equilibrium chosen for this illustration does not have a pronounced Shafranov shift as would be produced in a higher beta, or higher poloidal beta plasma. Therefore, the peak in the current profile is not shifted to a large value of R. Instead, the profile is more ordinary with a relatively broad shape expected in a ST (lower A) [10, 29]. In this case the internal inductance $l_\mathrm{i} = 0.848$ and typically for these MAST plasmas it can be even lower, down to 0.6, as will be shown.

Finally, because the Thomson scattering measurements span the full cross section of the plasma, they can be used to examine if, as expected, the T_e profile is a flux function due to the high electron mobility in the plasmas. Figure 10 shows the Thomson measurements of electron temperature mapped onto the normalized psi of the kinetic plus MSE reconstruction. In blue are the measurements on the inboard side and in red those on the outboard side. If the electron temperature is a flux function, and the equilibrium is free of non-axisymmetric effects, these two sides should align. In this case they are quite close. It is possible to use a flux isotherm constraint in EFIT to enforce this condition [29], and in fact this will be required for reconstructions with rotation, but we have not as yet used that constraint here.

5. Initial analysis of the MAST database

In addition to the single equilibrium examples for MAST shown in the previous subsections, we have performed the same kinetic reconstruction analysis (with MSE) on many other discharges from the M7 (June 2008–March 2010) and M8 (May 2011–January 2012) experimental campaigns on MAST. Compiling an extensive database of kinetic equilibrium reconstructions from the MAST database is valuable for many reasons. For example, they can be used as partial input for a neural network to predict density and pressure profile shapes [37], or in the DECAF code [38] database of

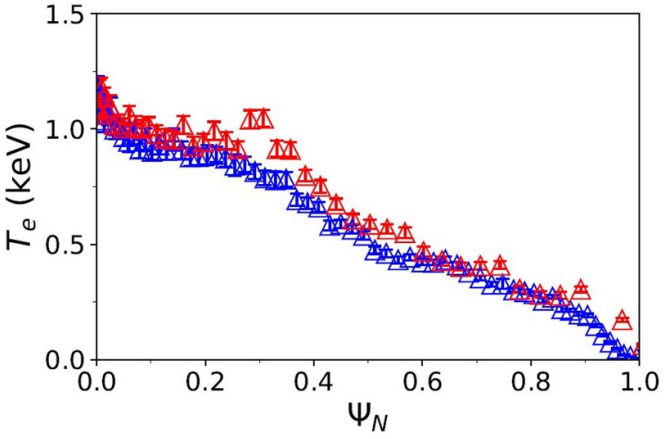

Figure 10. Thomson scattering T_e profile vs. normalized Ψ for MAST discharge 23890 at 0.269 s, showing measurements on the inboard side ($R < 0.97$ m) in blue, and the outboard side ($R > 0.97$ m) in red.

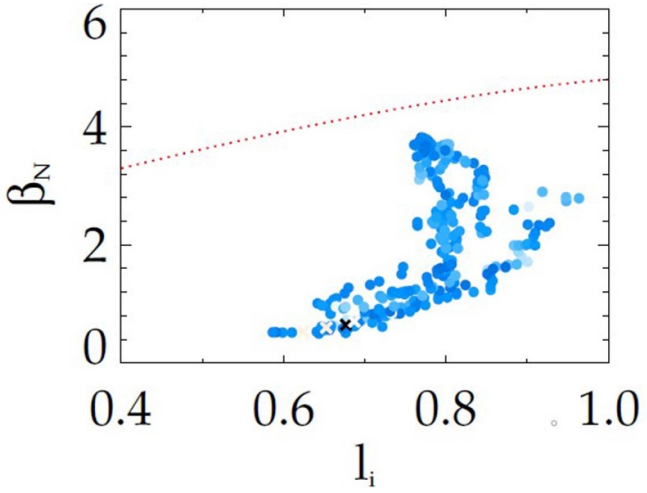

Figure 11. The calculated β_N vs. l_i stability space of plasmas in MAST. The blue colours indicate that nearly all equilibria have positive δW, below the no-wall limit. The dashed red line is the neural-net determined no-wall limit for NSTX.

multiple machine plasma disruptions. Additionally, a database of MAST equilibria will be useful to perform stability calculations of various types, including supplying input to a machine learning analysis of ideal MHD stability [3].

The ideal stability of MAST plasmas has been studied for individual or handfuls of discharges before [3, 8, 39, 40]; the utility here is in compiling a large database. The no-wall beta limit has been explored for projected plasmas in MAST-U through artificial scans of pressure and q profiles [4]. Here, the MAST database provides a natural scan of parameter space, rather than relying on theoretical scans that create combinations of profiles that may never be physically accessed in experiments. Even though it does not provide the full picture of global plasma stability [41], ideal stability calculations, for example knowledge of the no-wall beta limit, are important for tokamak operations, as they can be indicative of other plasma stability issues as well [42].

In the present work we will utilize the newly constructed database of MAST kinetic equilibrium reconstructions to test the capability of the DCON code [43] to determine the ideal stability of MAST plasmas. Ten different MAST discharges were used (23822, 23843, 23890, 24040, 24065, 24175, 24204, 24306, 24408, 24455). The kinetic equilibria with MSE generated in EFIT for these discharges were first fed through the CHEASE flux-coordinate code [44] which is implemented to further increase the numerical accuracy of the solution of the Grad–Shafranov equation. The CHEASE output was then read in DCON, which determines the change in potential energy, δW, a negative value of which indicates the plasma is above the no-wall ideal toroidal mode number $n = 1$ MHD stability limit. Within each discharge the β_N tended to increase with time and the pressure profile peaking decreased, but unfortunately q_0 also tended to decrease with time often going below 1 for the higher β_N portions of the discharge. Since $q_0 < 1$ leads to DCON showing internal, rather than global mode instability, these times were discarded, leaving 275 time points between the ten discharges.

Figure 11 shows the resulting calculations of the 275 equilibria plotted on a β_N vs. l_i plot (the values of β_N and l_i are taken from DCON after the CHEASE processing, but they are nearly identical to the underlying EFIT-determined values). The colour of the points indicates their value of δW, with darker blue circles being more positive (more stable), lighter blue less stable, and red x's would indicate instability (see, for example, figure 1 from [41] for NSTX). In this case, however, practically all the points are stable, except for a couple of very light x's indicating a few calculations barely over the limit. This is not actually unexpected for MAST; in MAST the wall stabilization was quite weak, so the ideal *with*-wall limit was thought to be barely above the no-wall limit [4], and the practical implication of that was that plasmas in the MAST database should have very sparsely sampled the wall stabilized region of stability space. The dashed red line in figure 10 is the no-wall limit determined by a neural network for NSTX which showed possible indications of being useful for MAST as well [3]. All the equilibria calculated so far are below this limit. Specific effort will be required in future work to find MAST discharges in the database that can be used to refine the stability limit for MAST (higher β_N with $q_0 > 1$), but this initial study indicates that the kinetic equilibrium reconstructions produced so far are of sufficient quality for trustworthy stability calculations and are shown to be ideal MHD stable for $n = 1$ global MHD modes.

6. Preparation for equilibrium reconstruction of the first plasmas in MAST-U

The upgrade to MAST [2] was motivated by a desire to increase the plasma pulse length, heating power, current, and magnetic field, as well as to introduce a new advanced divertor configuration [45]. Naturally, these changes required changes to the machine, which means that the conducting structure in

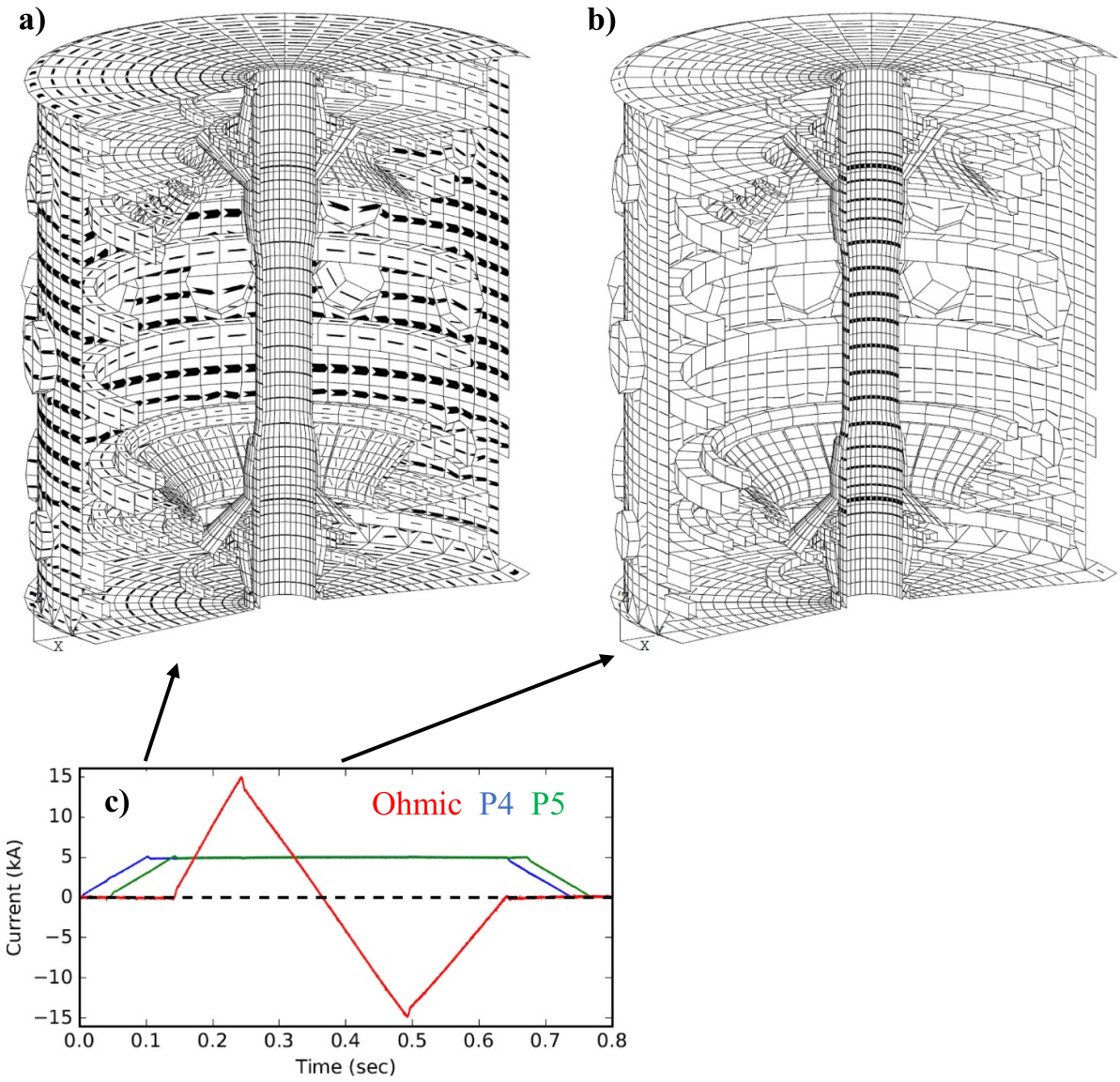

Figure 12. Views of the eddy current pattern in the MAST-U conducting structure during vacuum test discharge 41223 at (a) 0.1 s, and (b) 0.4 s. Panel (c) shows the currents in the Ohmic (red), P4 (blue), and P5 (green) coils.

MAST-U is substantially different from that of MAST in several ways. Already it has been shown that the new conducting structure, in particular the stainless steel passive stabilisation plates (PSP), can impact the stability of the plasmas [4], as well as the start-up scenarios for plasma breakdown [46]. Of course, they will also impact reconstruction of the equilibrium. Like the VALEN model of the conducting structure used for MAST, the model for MAST-U is fully 3D, including all the ports in the vacuum vessel [4]. In the actual equilibrium reconstructions, also as in the MAST case, the vessel structures with estimated current are a reduced axisymmetric set of the structure. In figure 4(b), the MAST-U conducting structure was shown in the same way as discussed for MAST in section 3. Note that the poloidal field coils [47] and magnetic diagnostics [48] have changed as well. Also, like in the MAST case, VALEN is used to determine eddy currents in the 3D vessel structures for vacuum coil test shots. A diagram of the MAST-U conducting structure in VALEN [4], similar to figure 2 for MAST, is shown in figure 12. For MAST-U vacuum test discharge 41223, the Ohmic, P4, and P5 coils were tested, using the currents shown in figure 12(c). At 0.1 s, during the P4 and P5 ramps, and before the Ohmic coil has current, the induced currents are mainly in the outer vacuum vessel and also the P4 and P5 coil cases (figure 12(a)). The total toroidal current in the vacuum vessel reaches about 90 kA. Later, at 0.4 s, during the P4 and P5 flattops and during the Ohmic current swing, currents totalling almost 90 kA are induced almost exclusively in the centre stack casing (figure 12(b)). In the plots, the arrows in each element are proportional to the current in that element, but they are rescaled between the time points so the largest arrow fits inside its element. There is almost twice as much current in the centre stack casing in the second plot as there is in the whole vessel in the first plot.

Like in the MAST case, the VALEN currents are mapped to effective resistances in the two-dimensional (2D) vessel

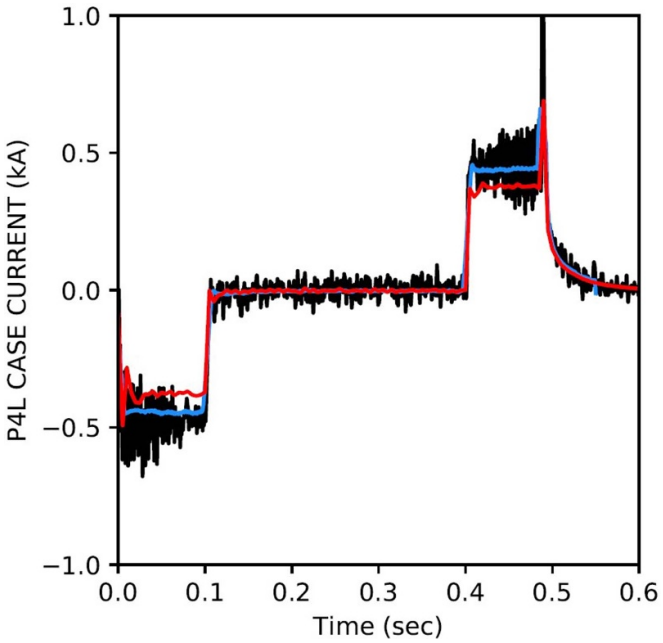

Figure 13. Comparison between measured (black) and VALEN (red) and EFIT++ (blue) modelled induced currents in the lower P4 coil case during MAST-U poloidal field coil test discharge 40315.

groupings in EFIT to be used in conjunction with nearby loop voltage measurements for estimated currents in the structures during reconstruction. In addition to the 3D VALEN model used in conjunction with the EFIT implementation of the present work, the EFIT++ code, which will also be used for MAST-U reconstructions, contains its own 2D conducting structure model.

First, analogously to figure 3 for MAST, the VALEN and EFIT++ models are tested by comparing between the modelled current in the coil cases and the measured current from Rogowski coils. Figure 13 shows this comparison, again for the P4 lower case, for MAST-U vacuum test discharge 40315, in which only the P4 coil was energized. As in figure 3, the noise in the measured signal is due to it being the difference between two large signals, the Rogowski measurements of the coil plus case currents minus the coil feed current. The comparison shows adequate, if not perfect, agreement, which should improve with further test discharges. This gives enough confidence in the models to again proceed to compare the conducting vessel segments shown in figure 4 with loop voltage measurements in order to determine effective resistances to use for equilibrium reconstructions.

Here, the PSP are again of particular interest because they are a new non-axisymmetric 3D structure that is quite close to the plasma surface. The connections between the individual plates span only half the plates height (see figure 14), and the resistivity of those connections is modelled, but not precisely known. If there is notable extra resistance due to the mechanical joint from plate to plate, eddy currents will be more likely to circulate within each plate. In other words, there will be a large current without a net toroidal component within each plate. On the other hand, if there is negligible

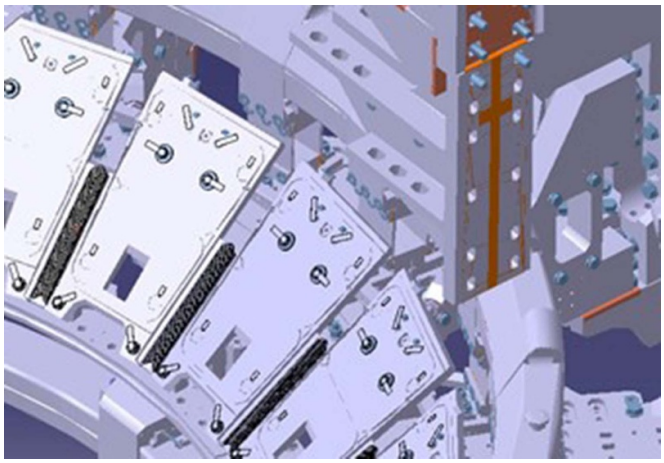

Figure 14. Diagram of the passive stabilization plates (PSP) in MAST-U, showing the gaps and connections between individual plates.

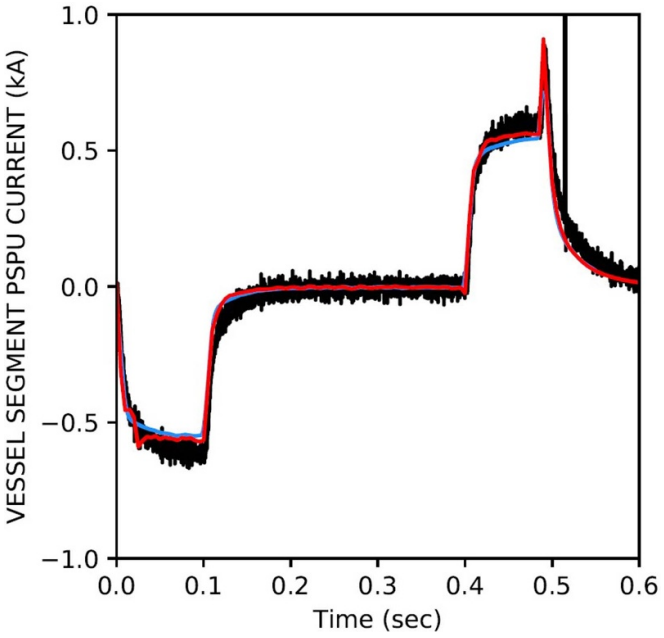

Figure 15. Comparison between measured loop voltage divided by effective resistance (black) and VALEN (red) and EFIT++ (blue) modelled induced currents in the upper passive stabilization plate structure during MAST-U poloidal field coil test discharge 40315.

extra resistance due to the mechanical joint (plate to plate) the sum total of all plates will act as a complete toroidal conductive path. This effect will be most important for periods of transient coil currents, less so at steady state. The effective resistance of the 2D EFIT vessel structure group that contains these actually 3D structures must be calibrated to accurately capture the effective 2D axisymmetric current resulting from the modelled 3D behaviour. The eddy current paths that show a reversal of the current toroidally can be reconstructed by EFIT if the PSP model is set up to allow this. Such a result has been shown for the copper passive conducting plates in NSTX.

Figure 15 shows the comparison between the modelled induced currents in the upper passive stabilization plate structure during MAST-U poloidal field coil test discharge 40315, and a nearby loop voltage measurement divided by an effective resistance which is chosen so that current matches the VALEN model. This demonstrates that the VALEN model, as implemented, is able to capture the response of the PSP structures.

7. Conclusions

The necessary preparations for kinetic plasma equilibrium reconstructions are now established for the first operation of the MAST-U device. The 3D conducting structure has been implemented in the VALEN code and tested, demonstrating readiness for vessel current inclusion in MAST-U reconstructions. The technique of using VALEN to determine eddy currents in the vessel structures during vacuum coil test shots and then using these to estimate currents in grouped vessel structures during the reconstruction of plasma discharges has been successfully established for a large database of discharges from MAST operation. Kinetic equilibrium reconstructions have been performed for this database in three levels: with magnetic measurements only, with magnetics and Thomson scattering measurements of electron temperature and density, charge exchange recombination spectroscopy measurements of ion temperature, and finally with those plus MSE diagnosis of internal magnetic field pitch angle. The pitch angle data corroborates, but does not substantially change, the kinetic reconstructions analysed to date. Very low convergence errors were obtained for all discharges typically by the point in the current ramp-up when 50% of the full target plasma current was reached or certainly once the NBI power was applied and the plasma stored energy began to increase above the order of a few kJ (the NBI turn on came at various times, from during the ramp-up to well into the flat-top, in MAST discharges). Finally, the database of 275 MAST kinetic equilibrium reconstructions was used in DCON to calculate the ideal MHD stability in MAST. All discharges tested so far were below the $n = 1$ no-wall limit; further analysis is underway to examine the database further.

Data availability statement

The data that support the findings of this study are available upon reasonable request from the authors.

Acknowledgments

The authors acknowledge the invaluable help of R Akers, L Guazzotto, N Hawkes, J Hollocombe, A Kirk, A Piccione, D Taylor, and A Thornton. This research was supported by the U.S. Department of Energy under contracts DE-SC0018623 (Columbia University), and DE-AC02-09CH11466 (PPPL). This work is also partly funded by the RCUK Energy Programme (Grant No. EP/T012250/1) (CCFE) and by the Engineering and Physical Sciences Research Council [EP/L01663X/1] (Durham University). To obtain further information on the data and models underlying this paper please contact PublicationsManager@ukaea.uk.

ORCID iDs

J W Berkery https://orcid.org/0000-0002-8062-3210
D Ryan https://orcid.org/0000-0002-7735-3598
Y Jiang https://orcid.org/0000-0003-3252-8910
D J Battaglia https://orcid.org/0000-0001-8897-9740
C Ham https://orcid.org/0000-0001-9190-8310

References

[1] Harrison J R *et al* 2019 *Nucl. Fusion* **59** 112011
[2] Milnes J, Ayed N B, Dhalla F, Fishpool G, Hill J, Katramados I, Martin R, Naylor G, O'Gorman T and Scannell R 2015 *Fusion Eng. Des.* **96** 42
[3] Piccione A, Berkery J W, Sabbagh S A and Andreopoulos Y 2020 *Nucl. Fusion* **60** 046033
[4] Berkery J W, Xia G, Sabbagh S A, Bialek J M, Wang Z R, Ham C J, Thornton A and Liu Y Q 2020 *Plasma Phys. Control. Fusion* **62** 085007
[5] Sabbagh S A *et al* 2001 *Nucl. Fusion* **41** 1601
[6] Storrs J, Dowling J, Counsell G and McArdle G 2006 *Fusion Eng. Des.* **81** 1841
[7] Eidietis N W, Gerhardt S P, Granetz R S, Kawano Y, Lehnen M, Lister J B, Pautasso G, Riccardo V, Tanna R L and Thornton A J 2015 *Nucl. Fusion* **55** 063030
[8] Hole M J *et al* 2005 *Plasma Phys. Control. Fusion* **47** 581
[9] Chapman I T, Hua M-D, Pinches S D, Akers R J, Field A R, Graves J P, Hastie R J and Michael C A 2010 *Nucl. Fusion* **50** 045007
[10] Von Nessi G T, Hole M J, Svensson J and Appel L 2012 *Phys. Plasmas* **19** 012506
[11] Budny R V *et al* 1992 *Nucl. Fusion* **32** 429
[12] Field A R, Michael C, Akers R J, Candy J, Colyer G, Guttenfelder W, Ghim Y-C, Roach C M and Saarelma S 2011 *Nucl. Fusion* **51** 063006
[13] Van Wyk F, Highcock E G, Field A R, Roach C M, Schekochihin A A, Parra F I and Dorland W 2017 *Plasma Phys. Control. Fusion* **59** 114003
[14] Cecconello M, Boeglin W, Keeling D, Conroy S, Klimek I and Perez R V 2019 *Nucl. Fusion* **59** 016006
[15] Lao L L, St. John H, Stambaugh R D, Kellman A G and Pfeiffer W 1985 *Nucl. Fusion* **25** 1611
[16] Lao L L, Ferron J R, Groebner R J, Howl W, St. John H, Strait E J and Taylor T S 1990 *Nucl. Fusion* **30** 1035
[17] Lao L L, John H E S, Peng Q, Ferron J R, Strait E J, Taylor T S, Meyer W H, Zhang C and You K I 2005 *Fusion Sci. Technol.* **48** 968
[18] McArdle G J and Taylor D 2008 *Fusion Eng. Des.* **83** 188
[19] Appel L *et al* 2006 A unified approach to equilibrium reconstruction *33rd EPS Conf. on Plasma Physics* (*Rome, 19–23 June 2006*) vol 30I p 2.184
[20] Appel L and Lupelli I 2018 *Comput. Phys. Commun.* **223** 1
[21] Strait E J, Fredrickson E D, Moret J-M and Takechi M 2008 *Fusion Sci. Technol.* **53** 304
[22] Edlington T, Martin R and Pinfold T 2001 *Rev. Sci. Instrum.* **72** 421
[23] Scannell R, Walsh M J, Dunstan M R, Figueiredo J, Naylor G, O'Gorman T, Shibaev S, Gibson K J and Wilson H 2010 *Rev. Sci. Instrum.* **81** 10D520
[24] Gibson K J *et al* 2010 *Plasma Phys. Control. Fusion* **52** 124041

[25] Conway N J, Carolan P G, McCone J, Walsh M J and Wisse M 2006 *Rev. Sci. Instrum.* **77** 10F131
[26] Patel A, Carolan P G, Conway N J and Akers R J 2004 *Rev. Sci. Instrum.* **75** 4944
[27] Carpanese F, Felici F, Galperti C, Merle A, Moret J M and Sauter O 2020 *Nucl. Fusion* **60** 066020
[28] Boyer M D, Kaye S and Erickson K 2019 *Nucl. Fusion* **59** 056008
[29] Sabbagh S A *et al* 2006 *Nucl. Fusion* **46** 635
[30] Conway N J, De Bock M F M, Michael C A, Walsh M J, Carolan P G, Hawkes N C, Rachlew E, McCone J F G, Shibaev S and Wearing G 2010 *Rev. Sci. Instrum.* **81** 10D738
[31] De Bock M F M, Citrin J, Saarelma S, Temple D, Conway N J, Kirk A, Meyer H and Michael C A 2012 *Plasma Phys. Control. Fusion* **54** 025001
[32] Fitzgerald M, Appel L C and Hole M J 2013 *Nucl. Fusion* **53** 113040
[33] Guazzotto L, Betti R, Manickam J and Kaye S 2004 *Phys. Plasmas* **11** 604
[34] Guazzotto L and Betti R 2015 *Phys. Plasmas* **22** 092503
[35] Liu Y Q, Kirk A, Lyons B C, Munarretto S, Paz-Soldan C, Piron L and Turnbull A D 2020 *Nucl. Fusion* **60** 096026
[36] Bialek J M, Boozer A H, Mauel M E and Navratil G A 2001 *Phys. Plasmas* **8** 2170
[37] Boyer M D and Chadwick J 2021 *Nucl. Fusion* **61** 046024
[38] Berkery J W, Sabbagh S A, Bell R E, Gerhardt S P and LeBlanc B P 2017 *Phys. Plasmas* **24** 056103
[39] Chapman I T *et al* 2011 *Nucl. Fusion* **51** 073040
[40] Chapman I T, Gryaznevich M P, Howell D F and Liu Y Q 2011 *Plasma Phys. Control. Fusion* **53** 065022
[41] Berkery J W, Sabbagh S A, Bell R E, Gerhardt S P, LeBlanc B P and Menard J E 2015 *Nucl. Fusion* **55** 123007
[42] Piovesan P *et al* 2017 *Plasma Phys. Control. Fusion* **59** 014027
[43] Glasser A H 2016 *Phys. Plasmas* **23** 072505
[44] Lutjens H, Bondeson A and Sauter O 1996 *Comput. Phys. Commun.* **97** 219
[45] Morris W, Harrison J R, Kirk A, Lipschultz B, Militello F, Moulton D and Walkden N R 2018 *IEEE Trans. Plasma Sci.* **46** 1217
[46] Battaglia D J, Thornton A J, Gerhardt S P, Kirk A, Kogan L and Menard J E 2019 *Nucl. Fusion* **59** 126016
[47] McArdle G J, Pangione L and Kochan M 2020 *Fusion Eng. Des.* **159** 111764
[48] Piron L *et al* 2020 *Fusion Eng. Des.* **161** 111932